Inducing Immune Response with FLASH and Conventional Radiation in Diffuse Midline Glioma (DMG)

Oscar Padilla MD[1,15#], Hanna E. Minns BS[2#], Hong-Jian Wei PhD[1], Andrea Webster-Carrion MD[2], Masih Tazhibi BS[1], Nicholas M. McQuillan BS[1], Xu Zhang PhD[2,3,4], Matthew Gallitto, MD[1], Rebecca Yeh BS[2], Zhiguo Zhang PhD[2,3,4], Tom K. Hei PhD[1,5], Luca Szalontay MD[2], Jovana Pavisic MD[2], Guy Garty PhD[1,5,6], James H. Garvin MD PhD[2], Peter D. Canoll MD PhD[7], Claire Vanpouille-Box PhD[8], Vilas Menon PhD[9,10,11], Marta Olah PhD[9,11], Raul Rabadan PhD[12,13,14], Cheng-Chia Wu MD PhD[1], Robyn D. Gartrell MD MS[2*]

[#]denotes equal contribution

[*]**corresponding author:** Robyn Gartrell, Department of Pediatrics, Columbia University Irving Medical Center, New York, NY, USA. rdg2129@cumc.columbia.edu.

[1]Department of Radiation Oncology, Columbia University Irving Medical Center, New York, NY

[2]Department of Pediatrics, Columbia University Irving Medical Center, New York, NY

[3]Institute for Cancer Genetics, Columbia University Irving Medical Center, New York, NY

[4]Department of Genetics and Development, Columbia University Irving Medical Center, New York, NY

[5]Center for Radiological Research, Columbia University Irving Medical Center, New York, NY

[6]Radiological Research Accelerator Facility, Columbia University Irving Medical Center, Irvington, NY.

[7]Department of Pathology and Cell Biology, Columbia University Irving Medical Center, New York, NY

[8]Department of Radiation Oncology, Weill Cornell Medicine, New York, NY

[9]Department of Neurology, Columbia University Irving Medical Center, New York, NY

[10]Center for Translational and Computational Neuroimmunology, Columbia University Irving Medical Center, New York, NY

[11]Taub Institute for Research on Alzheimer's Disease and the Aging Brain, Columbia University Irving Medical Center, New York, NY

[12]Department of Systems Biology, Columbia University Irving Medical Center, New York, NY

[13]Department of Biomedical Informatics, Columbia University Irving Medical Center, New York, NY

[14]Program for Mathematical Genomics, Columbia University Irving Medical Center, New York, NY

[15]Department of Radiation Oncology, Icahn School of Medicine at Mount Sinai, New York, NY

Running title: Radiation effect on DMG immune microenvironment

Keywords: FLASH, radiation, diffuse midline glioma, DMG, DIPG, tumor microenvironment, immune modulation, genome biology, single cell technologies

Funding

This project was funded by the Hyundai Hope on Wheels Hope Scholar Award (PI: R.D.G, Grant #716838) and Swim Across America, including salary support for R.D.G and H.E.M. O.P. received support from the NCI Stimulating Access to Research in Residency (StARR) Award, supplement to the Columbia Cancer Research Program for Resident Investigators (R38CA231577). C-C.W received support from Gary and Yael Fegel Family Foundation (CU21-1080), St. Baldrick's Foundation (SBF CU21-0529), the Star and Storm Foundation, Sebastian Strong Foundation, and the Matheson Foundation (UR010590). Development of the FLASH irradiator was partially supported by NIAID Grant U19-AI067773 and by the Departments of Radiation Oncology at Columbia University Irving Medical Center and Weill Cornell Medical Center, as well as by an unrestricted research gift from Barry Neustein. Studies in ZZ laboratory is supported by NINDS (NS 132344). This study used Shared Resources of the Herbert Irving Comprehensive Cancer Center (HICCC) funded in part through Center Grant P30CA013696, specifically Molecular Pathology, Flow Cytometry, Oncology Precision Therapeutics and Imaging (OPTIC), and Genomics and High Throughput Screening Shared Resources. The content is solely the responsibility of the authors and does not necessarily represent the official views of the NIH.

Acknowledgements

We would like to thank Dr. Oren J. Becher for providing the murine DIPG 4423 cell line, and Jim Sharkey, Ron Drake and James Viera for their assistance with the FLASH irradiator including Clinac setup and maintenance. Additionally, we would like to thank Drs. Yuewen Tan and Naresh Deoli who helped with FLASH irradiation experiments.

Conflict of Interest Statement

We have no declarations to report.

Data Sharing Statement

Data available upon request to corresponding author Dr. Robyn Gartrell.

Statistics

Dr. Robyn Gartrell (rdg2129@cumc.columbia.edu) is responsible for all statistical analyses.

ABSTRACT

Purpose

Diffuse Midline Glioma (DMG) is a fatal tumor traditionally treated with radiotherapy (RT) and previously characterized as having a non-inflammatory tumor immune microenvironment (TIME). FLASH is a novel RT technique using ultra-high dose-rate, which is associated with decreased toxicity and effective tumor control. However, the effect of radiation effect on the DMG tumor immune microenvironment (TIME) has not yet been explored.

Methods

Here, we perform single-cell RNA sequencing and flow cytometry on immune cells isolated from an orthotopic syngeneic murine model of brainstem DMG following the use of FLASH (90Gy/sec) or conventional (2Gy/min) dose-rate RT (CONV), and compare to unirradiated tumor.

Results

FLASH exerts similar effects as CONV in the predominant microglial population, including the presence of two activated subtypes. In non-resident myeloid clusters of macrophages and dendritic cells, we find increased type 1 interferon (IFN1) pathway enrichment for CONV compared to FLASH and tumor by scRNA-seq. We observe a similar trend by flow cytometry at day 4 post-RT with IFNAR+, while differences in overall immune cell proportions are insignificant at this timepoint. At day 10 post-RT, flow cytometry shows no difference in IFNAR+ between FLASH and CONV in infiltrating immune cells studied.

Conclusion

Our work is the first to map CONV and FLASH immune alterations of the DMG TIME with single-cell resolution. We find that FLASH ignites a temporally distinct but effective immune response while maintaining equal tumor control as CONV.

INTRODUCTION

Diffuse Intrinsic Pontine Glioma (DIPG), re-classified by the World Health Organization (WHO) in 2021 as Diffuse Midline Glioma, H3K27M-altered (DMG), is a universally fatal pediatric brain tumor that carries a median survival of 9 to 11 months.[1 2] While radiotherapy (RT) is the standard-of-care treatment for DMG, it only offers a 3 month improvement in survival.[3 4] Clinical trials have explored a variety of targeted therapies in combination with RT, yet none have prolonged survival.[4 5].

Combining immunotherapy with RT has improved survival in several adult cancers.[6-9] However, immunotherapies like immune checkpoint inhibitors have had minimal success in childhood malignancies and combination approaches with RT have not been tried in DMG.[10] In order to appropriately pursue combination strategies in DMG, we must first understand how RT affects the tumor immune microenvironment (TIME). This is particularly important in brainstem DMG for two main reasons. First, DMG has been shown to harbor an immunologically "cold" or non-inflammatory TIME) compared to adult glioblastoma, which makes the use of immunotherapy difficult and likely arises from the need to protect the brainstem and its cardiopulmonary regulatory functions from overwhelming inflammation.[11 12] Second, due to this precarious tumor location, evaluation of the DMG TIME after RT has not been studied, leaving a critical gap in determining immune responses that may be leveraged in combination with immunotherapy. Additionally, considering the importance of minimizing toxicity in this population, we must also evaluate novel RT approaches that may spare normal tissue while maintaining an adequate immune response.

FLASH, or ultra-high dose-rate RT (>40Gy per second), is a novel technique that demonstrates normal tissue sparing without compromising tumor control when compared to conventional

(CONV) dose-rate RT (≤2Gy per minute).[13-18] Specifically, FLASH has been associated with less neurocognitive toxicity compared to CONV, which is critical when considering RT in pediatric brain tumors.[13 19] RT at CONV dose-rates has been shown to effectively increase the antigenicity of tumor cells via type 1 interferon (IFN1) response and T-cell recruitment.[20 21] However, CONV can also deplete immune populations and induce regulatory T-cell phenotypes in the TIME.[22 23]. While immune studies are limited with FLASH, previous evidence suggests that when compared to CONV, ultra-high dose-rates yield higher $CD8^+$ T-cells and myeloid subsets in the TIME of a Lewis lung carcinoma model. Studies evaluating FLASH in the brain of non-tumor bearing mice find decreases in microglial activation and neuroinflammation when compared to CONV.[24-26] Moreover, a recent study evaluating proton FLASH in rat glioblastoma found that CONV and FLASH equally increase non-resident immune responses in the TIME when compared to untreated tumor at day 8 post-RT.[27] Notwithstanding this early evidence, immune responses post-RT in the DMG TIME have not yet been evaluated.

We use single cell RNA sequencing (scRNA-seq) and flow cytometry to analyze the TIME in an immunocompetent syngeneic orthotopic murine model of brainstem DMG post CONV or FLASH and compare to unirradiated tumor and normal brainstem. Our work is the first to map CONV and FLASH immune alterations in the DMG TIME.

METHODS

DMG tumor induction

We utilized a syngeneic murine brainstem DMG cell line (PDGFB+, H3.3K27M, $p53^{-/-}$ cell line, 4423 DIPG, Supplemental Methods).[28] All animal experiments were performed in accordance with national guidelines and approved by our Institutional Animal Care and Use Committee (IACUC).

Juvenile 5-week-old immunocompetent male B6(Cg)-Tyrc-2J/J mice were purchased from Jackson Laboratories (Bar Harbor, ME). At 6 weeks of age, mice were anesthetized with isoflurane, immobilized in the stereotactic instrument (Stoelting, Wood Dale, IL, USA), and underwent orthotopic brainstem implantation with 4423 DIPG at 100,000 cells per microliter (uL) per mouse. Tumors were confirmed 10 days post injection (dpi), using MRI (Supplemental Methods).

Radiation

At 17 dpi, tumor-bearing mice were randomly assigned to receive 15Gy of radiation either at a conventional dose-rate (CONV, 2 Gy/min) or at an ultra-high dose-rate (FLASH, 90 Gy/sec) using the Ultra-High Dose-Rate FLASH irradiator at our experimental irradiator facility, based on a repurposed Varian Clinac 2100C.[29] Mice were anesthetized using isoflurane and immobilized using a device incorporating 6.4mm thick adjustable lead shielding, which was aligned to external anatomy creating an open field around the mouse hindbrain (Supplemental Figure 1). All irradiations were performed using 9 MeV electrons (R_{50}=3.9 cm). Further details of radiation methods including beam parameters can be found in Supplemental Methods.

Experimental design and clustering of CD45+ immune cells

Mice were evaluated among four groups: CONV (15Gy at 2Gy/min), FLASH (15Gy at 90Gy/sec), no radiation (Tumor), or normal, healthy mice (Normal Brainstem). Four mice were studied per group for a total of 16 mice. Four days post-RT and 21 dpi, mice were euthanized and brainstems collected for hashtag scRNA-seq (Figure 1a) after CD45 isolation to focus on the immune population. Flow cytometry was also performed on the CONV, FLASH, and Tumor groups at day 4 (D4) and day 10 (D10) post-RT, following the same experimental protocols.

Immune cell isolation and processing for scRNA-seq

At 21 dpi and D4 post-RT, mice were euthanized for CD45+ immune cell isolation and taken for sorted hashtag scRNA-seq. After tissue processing and homogenization (Supplemental Methods), the pellet was resuspended in a staining solution consisting of 7AAD viability solution (Biolegend, 420403), APC anti-mouse CD45 (Biolegend, 147708), and a TotalSeq-B anti-mouse hashtag antibody specific to treatment group (Biolegend; Normal Brainstem:155843, Tumor:155837, CONV:155833, FLASH:155831). The cells were stained for 15 minutes before resuspension in 0.3% BSA (Millipore Sigma, A2058) and transfer to our institution's Center for Translational Immunology (CCTI) core for CD45 sorting via the Influx cell sorter. The sorting was capped at 30,000 CD45+ cells per mouse and these cells were then brought for sequencing at our institution's Genome Center's Single Cell Analysis Core. Four samples, one sample from each treatment group, were loaded onto a single channel of a 10x Chromium chip. Viability of each sample was assessed to ensure an equal number of cells taken from each sample were included in the pooled sample with a total of 10,000 cells submitted for scRNA-seq (Supplemental Methods).

Flow Cytometry

Following the same tissue dissection, homogenization and isolation protocol as done for scRNA-seq, mice were euthanized at D4 post-RT (21 dpi) and D10 post-RT (27 dpi). Cells were stained with a total of 14 markers including 7AAD, CD45, CD11B, CD163, CD206, CD11C, MHC-II, CD3, CD8, CD4, GR1, TMEM119, CD19 and IFNAR1 (Supplemental Methods). Antibody combinations against the following targets were used to define cell types (Supplemental Figure 2): microglia (MG), CD45loCD11B+GR1-TMEM119+; macrophages (MACs), CD45hiCD11B+GR1-TMEM119-; myeloid derived suppressor cells (MDSCs),

CD45hiCD11B+GR1+TMEM119-; dendritic cells (DCs), CD45+CD11C+MHCII+; CD19+ B-cells, CD45hiCD11B-CD3-CD19+; T-Cells, CD45HiCD11B-CD3+; CD8+ T-Cells, CD45hiCD11B-CD3+CD8+CD4-; CD4+ T-Cells, CD45hiCD11B-CD3+CD8-CD4+. These antibody combinations were chosen based on previous studies.[30-32]

RESULTS

FLASH and CONV confer isoeffective DMG control

To assess the effect of CONV and FLASH on tumor control we evaluated tumor volume between pre- and post-RT timepoints using MRI and observed a significant decrease in tumor volume at day 7 post-RT after both CONV (p=0.006) and FLASH (p=0.0008) compared to untreated tumor (Supplemental Figure 2a). Further, we performed survival analysis and find no significant differences between groups (p=0.2995; Supplemental Figure 2b).

scRNA-seq identifies unique immune clusters in DMG TIME

Clustering of 33,308 CD45+ cells reveals 17 unique cell subsets (Figure 1b, Supplementary Data 1). We first analyze all clusters in total, agnostic to treatment. From this, we identify four clusters of MG denoted as MG1, MG2, MG3, and MG4. We find three clusters of non-resident myeloid cells including MACs, MONOs and DCs. Of the non-myeloid clusters, the most abundant is a mature B-cell subtype (BC2). The remaining cells are distributed amongst a T-cell cluster (TC), a neutrophil cluster (NEUT), a pre-B-cell cluster (BC1), and a natural killer cell cluster (NK). We also report a mixed population of proliferative cells in a cluster defined by *Mki67* positivity and another mixed population cluster of *S100b+* cells, likely consisting of astrocytes that bypassed CD45 sorting. Lastly, a group of erythrocytes are present based on hemoglobin gene expression

(RBC, as well as a cluster of low-quality cells (lq). For individual treatment groups, we examine the proportion of cells coming from each cluster against their total cell number and find variation between groups (Figure 1c, Supplementary Data 1). We perform key marker gene identification for each cell type using differential gene expression analysis, comparing each cluster against all other clusters. From this, we see that each cell type is defined by unique gene signatures and validated by presence of canonical markers (Figure 1d, Supplementary Data 2).

Immune compartment differences between RT and Tumor groups evolve over time

To confirm presence of immune phenotypes and evaluate proportional comparisons between treatment groups we performed flow cytometry D4 and D10 post-RT. The gating strategy can be found in Supplemental Figure 3 and all statistical comparisons can be found in Supplementary Data 3. Similar proportions of MG are found at D4 and D10 post-RT comparing CONV and FLASH to Tumor (Figure 2a). Further, with the exception of the CONV group in which we observe a significant decrease in MG fraction between D4 and D10 post-RT ($p=0.0317$), the MG compartment remains insignificantly changed between D4 and D10 post-RT in FLASH and Tumor groups. However, at D10 post-RT there are significantly fewer MG in CONV and FLASH treated groups compared to Tumor ($p=0.0339$ and $p=0.0109$, respectively, Figure 2a). MACs (Figure 2b) are not significantly different at D4 when comparing CONV and FLASH to Tumor. We show a significant fractional increase in MACs from D4 to D10 in the Tumor group ($p=0.0079$) while no significant changes are seen in D4 to D10 post-RT in the CONV or FLASH groups. Therefore, at D10 , compared to Tumor, MACs in CONV are significantly decreased ($p=0.0196$) while FLASH is trending to lower compared to Tumor ($p=0.0562$). With regards to the GR1+ myeloid-derived suppressor cells (MDSCs, Figure 2c) there is no significant difference in proportions at D4 in CONV or FLASH compared to Tumor. However, at D10, CONV and FLASH induce a significant

fractional increase relative to Tumor (p=0.0070 and p=0.0086, respectively), as Tumor decreases at D10 compared to D4 (p=0.0476). There are no significant inter- or intra-group differences at D4 or D10 for DCs (Figure 2d). When comparing T-cells (Figure 2e), we see a significant fractional decrease from D4 to D10 in the Tumor group (p=0.0079), which also demonstrates a significantly lower T-cell fraction relative to CONV and FLASH at D10 (p=0.0072 and p=0.0089 respectively). We see that these T-cell differences at D10 vary by subtype, with CD8+ T-cells significantly increasing between CONV and Tumor (p=0.0023; Figure 2f) and CD4+ T-cells significantly increasing in FLASH compared to both CONV and Tumor (p=0.0409 and 0.0055, respectively; Figure 2g). Finally, CD19+ B-cells (Figure 2h) are found to be trending downward from D4 to D10 in CONV (p=0.0556) as they are significantly increased in Tumor compared to both CONV and FLASH at D10 (p=0.0196 and p=0.0058, respectively).

MG annotation reveals four distinct subtypes via scRNA-seq

MG represent the predominant population on scRNA-seq. MG are defined by expression of canonical genes such as *P2ry12*, *Siglech* and *Tmem119*,[32 33] and resolve into four distinct subtypes (MG1, MG2, MG3, and MG4) based on unique gene sets (Figure 3a). Expression of homeostatic marker *P2ry12* decreases from MG1 to MG4, while expression of *Apoe*, a marker of MG activation, increases in the MG3 and MG4 subtypes (Figure 3b).[32 34] MG1 and MG2 share similar profiles (Supplementary Data 2). MG3 is enriched for multiple interferon genes such as *Ifit3* and *Isg15* (Figure 3c, Supplementary Data 2) while MG4 shows high expression of metabolism-associated genes such as *Lpl* (lipoprotein lipase) and *Fabp5* (fatty-acid binding protein) (Figure 3d, Supplementary Data 2). We ran the top 50 differentially expressed genes in MG3 through REACTOME for pathway analysis (Supplemental Methods), with the top 3 pathways consisting of interferon alpha/beta signaling, interferon signaling, and cytokine signaling (Supplemental

Figure 4a). We ran the top 50 genes from MG4 through REACTOME, with the most significant pathways consisting of neutrophil degranulation, interleukin-10 signaling, glucose metabolism, and iron uptake (Supplemental Figure 4b).

In Normal Brainstem, MG1 and MG2 account for the majority of MG (44.5% and 47.0% respectively), with less than 10% of cells present in MG3 and MG4 clusters (Figure 3e, f). With Tumor, there is an expansion of MG4 (30.8%) while MG3 (4.85%) is maintained at a similar proportion as in Normal Brainstem (Figure 3e, f). Upon irradiation with either CONV or FLASH, the MG3 cluster undergoes significant expansion (17.0% and 16.2% respectively), while MG4 experiences moderate reduction (26.7% and 22.3% respectively) compared to Tumor (Figure 3e, f).

FLASH and CONV induce similar MG subtypes and early IFN1 response

We next perform two individual analyses to identify genomic alterations uniquely induced by FLASH and by CONV relative to Tumor (FvT and CvT, respectively; Supplementary Data 4). We compare both the common and the different up- and down-regulated genes resulting from each analysis. For all MG clusters, both RT modalities upregulate DNA damage response genes associated with ionizing radiation (i.e. *Cdkn1a*, *Phlda3*, *Bax*) to a similar extent (Supplemental Figure 4c, e).[35 36] In MG1 and MG2, FLASH and CONV similarly downregulate innate immunity chemokines *Ccl9* and *Ccl6* compared to Tumor (Supplemental Figure 4c). In MG3, both RT interventions similarly downregulate *Ccl9* along with *Klf2* (Supplemental Figure 4e), a myeloid repressor of neuroinflammation.[37] In MG4, both RT groups similarly upregulate IFN1 genes such as *Isg15, Ifitm3*, and *Ifit3*, while decreasing expression of major histocompatibility complex (MHC) class II genes *H2-Aa* and *H2-Ab1* compared to Tumor (Supplemental Figure 4e). Regarding differential upregulation of genes, FLASH shows unique enrichment for *Apoe* (MG1,

MG3) and *Ccl12* (MG1, MG2), while CONV shows distinct increases in *Cd52, Ifi27l2a, Ccl2,* and *Cst7* in MG4 (Supplementary Data 4).

We then ran the most significant, upregulated common genes between FvT and CvT for each MG cluster through REACTOME and find pathways associated with cell cycle checkpoints and DNA damage response (Supplemental Figure 4d, f). For MG4 specifically, we also find upregulation of common pathways relating to interferon alpha/beta signaling and cytokine signaling (Supplemental Figure 4f). Using flow cytometry, we stained MG with IFNAR to evaluate IFN1 response. Representative IFNAR peak shifts for the relevant cell types can be found in Supplemental Figure 2 and all statistical comparisons can be found in Supplementary Data 3. We find that at D4, there is no significant difference in IFNAR+ MG between FLASH and CONV compared to tumor (Supplemental Figure 5a). At D10, the percentage of IFNAR+ MG decreases in the FLASH treated mice relative to CONV (p=0.0162) and Tumor (p=0.0403) with no significant differences in any group comparing D4 to D10 (Supplemental Figure 5a).

FLASH and CONV induce differential MAC and DC IFN1

We next examine the non-resident myeloid clusters: MONO, MAC, and DC, and find clear segmentation of gene signatures, with varying degrees of overlap in classical myeloid markers such as *Ccr2* and *Vim*[38 39], and MHC class II genes *H2-Ab1* and *Cd74* (Supplemental Figure 6a). Studying the cell density of these clusters within the non-resident myeloid compartment of each treatment group, we find treatment-specific differences (Supplemental Figure 6b-c). We next perform differential gene expression analysis within the MAC cluster between individual RT groups and Tumor (FvT and CvT; Supplementary Data 4). We find similarly upregulated genes associated with RT response (e.g. *Cdkn1a, Bax*, and *Phlda3*)[35 36] as well as similarly

downregulated genes associated with antigen presentation (e.g. *Cd74, H2-Eb1, H2-Aa, H2-Ab1*) (Figure 4a). We then analyze the genes that are specifically upregulated in either FvT or CvT but not the other. For CONV, the most upregulated genes compared to Tumor include *Isg15, Irf7, Ifit3, Ifit2, Tgfbi,* and *Tspo* (Figure 4b). For FLASH, the most upregulated genes are *Mrc1, Pf4, Lyve1* and *Cd163*. Mapping the average expression of these genes onto non-resident myeloid clusters, we find a dichotomy between CONV (*Isg15 and Ifit3 shown*) and FLASH-associated (*Pf4 and Mrc1 shown*) genes that mirrors their individual cell densities in the MAC cluster (Figure 4c). Considering that the genes enriched in the FLASH group may reflect a particular MAC subtype, we assessed CD163 and CD206 (Mrc1) on MACs by flow cytometry and find no significant differences between FLASH and CONV at D4 or D10 (Supplemental Figure 5b). Importantly, these CD163+CD206+ MACs increase at D10 compared to D4 in both CONV (p=0.0159) and FLASH (p=0.0079) while these cells are not seen at D4 or D10 in Tumor. Moreover, at D10, there are more CD163+CD206+ MACs in both CONV (p=0.0175) and FLASH (p=0.0025) compared to Tumor (Supplemental Figure 5b).

Next, given the increase in interferon-associated gene expression with CONV, we evaluate IFN1 response by single sample gene set enrichment (ssGSEA) analysis (Supplemental Methods) and find that CONV MACs have a significantly higher IFN1 score compared to FLASH and Tumor (both $p < 0.0001$; Figure 4d). By flow cytometry, we observe differentially higher IFNAR+ MACs at D4 in CONV vs FLASH that trends toward significance (p=0.066; Figure 4e); this difference disappears at D10 as both RT groups have a higher IFNAR+ MAC fraction compared to Tumor (CONV p=0.0058, FLASH p=0.0109). Further, while the fraction of IFNAR+ MACs remains similar between D4 and D10 for CONV, the FLASH fraction trends upward and the Tumor fraction significantly decreases at D10 (p=0.0556 and p=0.0079, respectively).

Lastly, we perform differential gene expression analysis in the DC cluster and find only a few genes that are differentially expressed in FvT (upregulated: *Clec4b1, Pid1;* downregulated: *Mdh2, Il1b, Cdk2ap2)* (Figure 5a, Supplementary Data 4). Conversely, CvT has many differentially expressed genes (Figure 5a), with a robust increase in IFN1 related genes such as *Isg15, Irf7, Ifit3,* and *Ifit2,* and significant enrichment of IFN1 score on ssGSEA compared to FLASH and Tumor (both $p<0.0001$; Figure 5b). We then perform flow cytometry (Figure 5c), and validate our ssGSEA findings, confirming higher IFNAR+ DCs at D4 in CONV vs FLASH and Tumor (both $p=0.0196$). The percent of IFNAR+ DCs decreases at D10 in CONV ($p=0.0079$) while FLASH and Tumor remain similar, resulting in no significant differences between treatment groups at D10 (Figure 5c).

Characterization of lymphocyte clusters

NK, T- and B-cell clusters are defined by canonical genes (Supplemental Figure 7a). On FvT and CvT analyses, we find that FLASH upregulates *Lck*, *Klf2, Sell, and Lef1* in T-cells relative to Tumor (Supplemental Figure 7b). These genes are not increased for CONV compared to Tumor. Evaluation by flow cytometry demonstrates higher IFNAR+ T-cells (subtype agnostic) in FLASH vs CONV at D4 only ($p=0.0381$; Supplemental Figure 7c). Assessing CD8+ T-cells, we see higher IFNAR+ by flow cytometry in CONV vs FLASH at D4 only ($p=0.0311$; Supplemental Figure 7d). Analysis of B-cells demonstrates BC2 cells are enriched for maturation marker *Ms4a1* and immunoglobulin genes (e.g., *Ighd, Iglc2*)[40] (Supplementary Data 2). There were few genes differentially enriched for FvT and none for CvT among BC2 cells (Supplementary Data 4). NK cell and BC1 proportions were less than 1% of cells across tumor groups and thus not suitable for differential expression analysis (Supplementary Data 1).

DISCUSSION

DMG is a fatal pediatric tumor in desperate need of novel approaches, including immunotherapy. However, previous work demonstrates a non-inflammatory TIME in human DMG, when compared to adult glioblastoma, at diagnosis, in the unirradiated setting.[11] While RT is known to trigger an anti-tumor immune response, this has not been studied in DMG due to the precarious location of this disease and paucity of clinical specimens post irradiation.[20-23] Our study offers a unique perspective into understanding the RT immune response of both CONV and FLASH in the DMG TIME, using preclinical models that mimic the pathology of human DMG.[28] Consistent with prior studies in other tumor models, including gliomas, we find that RT dose-rate does not impact DMG control.[15-18] Moreover, we find no survival benefit with either RT modality using a single 15Gy fraction, which is not unexpected considering the high biologically effective doses that are required in fractionated clinical dose schedules for human DMG.[3 4] A previous FLASH study performed in a glioblastoma model parallels this finding, with survival advantages only achieved upon the use of hypofractionated RT schedules.[15]

In our study, we employ scRNA-seq and find 4 unique subtypes of MG with comparable gene expression profiles between CONV and FLASH. In tumor groups, with or without RT, we see a phenotypic continuum from homeostatic MG1 and MG2 to more activated states in MG4, as depicted by the increasing expression gradients of *Apoe, Spp1, Lpl,* and *Fabp5,* and enrichment of interleukin-10 signaling, glucose metabolism and iron uptake pathways along this MG trajectory. The literature ascribes this spectrum of genes and metabolic pathways culminating in MG4 to disease- and injury-associated MG states.[34 41] Moreover, we see that following irradiation with either FLASH or CONV, an interferon-associated MG subtype emerges in MG3.[42] Interestingly, MG4 also manifests IFN1 pathway expression, suggesting disease-associated MG retain some

capacity for immune activation in the setting of RT. We evaluated overall IFNAR+ in MG by flow cytometry to assess IFN1 response, finding similar expression when comparing Tumor, CONV and FLASH. While previous work shows that FLASH activates MG less than CONV in non-tumor bearing mice, our work demonstrates that these two dose-rates activate MG to a similar extent in pontine DMG at D4 post-RT.[25 43]

Compared to MG, non-resident myeloid cells, including MACs, DCs and MONOs, compose less of the immune repertoire in DMG TIME and are found in similar proportions across Tumor, CONV and FLASH groups. However, these cell types harbor differentially expressed genes according to treatment group. First, MACs have increased expression of IFN1 related genes including *Isg15* and *Ifit3* and increased IFN1 score by ssGSEA in CONV compared to FLASH. We evaluated IFNAR expression on MACs by flow cytometry and find a trend toward significance when comparing CONV and FLASH at D4 post-RT. Interestingly, at D10 post-RT, this difference vanishes and both RT groups show increased IFNAR+ MACs compared to Tumor, indicating that IFN1 response in MACs may occur later with FLASH.

DCs are critical mediators of anti-tumor T-cell responses via induction of IFN1 post-RT.[20 21] By scRNA-seq, we find that CONV elicits a robust IFN1 response in DCs. Our flow cytometry data further shows that while the DC proportions remains similar across treatment groups at D4 post-RT, IFNAR+ DCs are indeed higher in CONV compared to both FLASH and Tumor. However, at D10 post-RT, we find the percent of IFNAR+ DCs to be similar across CONV, FLASH and Tumor, indicating that this response is short-lived and lost over time regardless of dose-rate.

Previous studies in non-glioma murine models show that FLASH yields higher CD8+ T-cells in subcutaneous Lewis lung carcinoma at 6hr post-RT and higher CD4+ and CD8+ T-cells in

orthotropic ovarian cancer at 96hr post-RT.[16 24] However, in DMG, we see no significant increase in T-cells between FLASH and CONV at D4 post-RT.[16 24 44] This may be due to the lympho-depleted state of the DMG TIME at baseline.[11] However, we do see that T-cells increase at D10 post-RT in both CONV and FLASH, and decrease in Tumor. Specifically, at D10 post-RT, CD4+ T-cells are increased in FLASH compared to CONV and Tumor, while CD8+ T-cells are increased in CONV compared to Tumor. By scRNA-seq, we find that FLASH significantly upregulates genes involved in T-cell activation (*Lck*) and trafficking (*Klf2*), which occurs on the background of higher central-memory (*Sell, Lef1, Klf2*) and naïve (*Sell, Lef1, Ccr7*) T-cell states.[45 46]

Our study has several limitations, including interrogation of the TIME at only two timepoints and use of a single fraction schedule. Additionally, we did not include irradiated non-tumor bearing brainstems, which would help to distinguish the immune response arising from irradiation of healthy versus tumor tissue. Future studies should consider inclusion of such control as the diffuse nature of DMG, as observed in our model, complicates the delimitation and separation of these tissues within a given specimen.

In summary, proportions of immune cell subsets are similar between CONV and FLASH. Importantly, both resident and non-resident immune cells in the DMG TIME are able to mount a post-RT IFN1 response, which is a critical feature of tumors that typically respond to immunotherapy.[21] This IFN1 response is equally seen between CONV and FLASH in MG. However, IFN1 is more frequently seen following CONV in non-resident myeloid cells, specifically in DCs and MACs. The latter observation highlights the opportunity to combine CONV with immunotherapies that leverage the non-resident myeloid compartment, which has been proposed for other tumors.[47-49] Although less of an IFN1 response is seen in the non-resident myeloid compartment with FLASH at D4 post-RT, this response increases and equalizes to CONV

by D10, implying that FLASH may provoke a delayed IFN1 response that occurs after the D4 scRNA-seq timepoint. The potential opportunity of this latent IFN1 response can be better understood in the context of excessive immune recruitment in the brainstem, which can be a double-edged sword as neuroinflammation in this area may be fatal and is associated with neurocognitive dysfunction in children.[50] Therefore, it is important to consider the effect of RT dose-rate on neuroinflammation in the brainstem, especially when combining with systemic and immune-based therapies for the treatment of DMG. Lastly, temporal immunogenicity associated with different RT dose-rates will be important to consider, and warrants future studies, to effectively and safely combine RT with immunotherapy in DMG.

REFERENCES

1. Cooney T, Lane A, Bartels U, et al. Contemporary survival endpoints: an International Diffuse Intrinsic Pontine Glioma Registry study. *Neuro Oncol* 2017;19(9):1279-80. doi: 10.1093/neuonc/nox107 [published Online First: 2017/08/20]
2. Louis DN, Perry A, Wesseling P, et al. The 2021 WHO Classification of Tumors of the Central Nervous System: a summary. *Neuro Oncol* 2021;23(8):1231-51. doi: 10.1093/neuonc/noab106
3. Johung TB, Monje M. Diffuse Intrinsic Pontine Glioma: New Pathophysiological Insights and Emerging Therapeutic Targets. *Curr Neuropharmacol* 2017;15(1):88-97. doi: 10.2174/1570159x14666160509123229
4. Theeler BJ, Dalal Y, Monje M, et al. NCI-CONNECT: Comprehensive Oncology Network Evaluating Rare CNS Tumors-Histone Mutated Midline Glioma Workshop Proceedings. *Neurooncol Adv* 2020;2(1):vdaa007. doi: 10.1093/noajnl/vdaa007 [published Online First: 2020/07/10]
5. Long W, Yi Y, Chen S, et al. Potential New Therapies for Pediatric Diffuse Intrinsic Pontine Glioma. *Front Pharmacol* 2017;8:495. doi: 10.3389/fphar.2017.00495 [published Online First: 2017/08/10]
6. Antonia SJ, Villegas A, Daniel D, et al. Durvalumab after Chemoradiotherapy in Stage III Non-Small-Cell Lung Cancer. *N Engl J Med* 2017;377(20):1919-29. doi: 10.1056/NEJMoa1709937 [published Online First: 2017/09/09]
7. Jabbour SK, Lee KH, Frost N, et al. Pembrolizumab Plus Concurrent Chemoradiation Therapy in Patients With Unresectable, Locally Advanced, Stage III Non-Small Cell Lung Cancer: The Phase 2 KEYNOTE-799 Nonrandomized Trial. *JAMA Oncol* 2021;7(9):1-9. doi: 10.1001/jamaoncol.2021.2301 [published Online First: 2021/06/05]
8. Burtness B, Harrington KJ, Greil R, et al. Pembrolizumab alone or with chemotherapy versus cetuximab with chemotherapy for recurrent or metastatic squamous cell carcinoma of the head and neck (KEYNOTE-048): a randomised, open-label, phase 3 study. *Lancet* 2019;394(10212):1915-28. doi: 10.1016/S0140-6736(19)32591-7 [published Online First: 2019/11/05]

9. Ma BBY, Lim WT, Goh BC, et al. Antitumor Activity of Nivolumab in Recurrent and Metastatic Nasopharyngeal Carcinoma: An International, Multicenter Study of the Mayo Clinic Phase 2 Consortium (NCI-9742). *J Clin Oncol* 2018;36(14):1412-18. doi: 10.1200/JCO.2017.77.0388 [published Online First: 2018/03/28]
10. Long AH, Morgenstern DA, Leruste A, et al. Checkpoint Immunotherapy in Pediatrics: Here, Gone, and Back Again. *Am Soc Clin Oncol Educ Book* 2022;42:1-14. doi: 10.1200/EDBK_349799
11. Lin GL, Nagaraja S, Filbin MG, et al. Non-inflammatory tumor microenvironment of diffuse intrinsic pontine glioma. *Acta Neuropathol Commun* 2018;6(1):51. doi: 10.1186/s40478-018-0553-x [published Online First: 2018/06/30]
12. Price G, Bouras A, Hambardzumyan D, et al. Current knowledge on the immune microenvironment and emerging immunotherapies in diffuse midline glioma. *EBioMedicine* 2021;69:103453. doi: 10.1016/j.ebiom.2021.103453 [published Online First: 2021/06/23]
13. Montay-Gruel P, Petersson K, Jaccard M, et al. Irradiation in a flash: Unique sparing of memory in mice after whole brain irradiation with dose rates above 100Gy/s. *Radiother Oncol* 2017;124(3):365-69. doi: 10.1016/j.radonc.2017.05.003 [published Online First: 2017/05/27]
14. Montay-Gruel P, Bouchet A, Jaccard M, et al. X-rays can trigger the FLASH effect: Ultra-high dose-rate synchrotron light source prevents normal brain injury after whole brain irradiation in mice. *Radiother Oncol* 2018;129(3):582-88. doi: 10.1016/j.radonc.2018.08.016 [published Online First: 2018/09/05]
15. Montay-Gruel P, Acharya MM, Goncalves Jorge P, et al. Hypofractionated FLASH-RT as an Effective Treatment against Glioblastoma that Reduces Neurocognitive Side Effects in Mice. *Clin Cancer Res* 2021;27(3):775-84. doi: 10.1158/1078-0432.CCR-20-0894 [published Online First: 2020/10/17]
16. Eggold JT, Chow S, Melemenidis S, et al. Abdominopelvic FLASH Irradiation Improves PD-1 Immune Checkpoint Inhibition in Preclinical Models of Ovarian Cancer. *Mol Cancer Ther* 2022;21(2):371-81. doi: 10.1158/1535-7163.MCT-21-0358 [published Online First: 2021/12/07]
17. Bertho A, Iturri L, Prezado Y. Radiation-induced immune response in novel radiotherapy approaches FLASH and spatially fractionated radiotherapies. *Int Rev Cell Mol Biol* 2023;376:37-68. doi: 10.1016/bs.ircmb.2022.11.005 [published Online First: 2023/03/31]
18. Velalopoulou A, Karagounis IV, Cramer GM, et al. FLASH Proton Radiotherapy Spares Normal Epithelial and Mesenchymal Tissues While Preserving Sarcoma Response. *Cancer Res* 2021;81(18):4808-21. doi: 10.1158/0008-5472.CAN-21-1500 [published Online First: 2021/07/30]
19. Montay-Gruel P, Acharya MM, Petersson K, et al. Long-term neurocognitive benefits of FLASH radiotherapy driven by reduced reactive oxygen species. *Proc Natl Acad Sci U S A* 2019;116(22):10943-51. doi: 10.1073/pnas.1901777116 [published Online First: 2019/05/18]
20. De Martino M, Padilla O, Daviaud C, et al. Exploiting Radiation Therapy to Restore Immune Reactivity of Glioblastoma. *Front Oncol* 2021;11:671044. doi: 10.3389/fonc.2021.671044 [published Online First: 2021/06/08]
21. Vanpouille-Box C, Alard A, Aryankalayil MJ, et al. DNA exonuclease Trex1 regulates radiotherapy-induced tumour immunogenicity. *Nat Commun* 2017;8:15618. doi: 10.1038/ncomms15618 [published Online First: 2017/06/10]
22. Yovino S, Kleinberg L, Grossman SA, et al. The etiology of treatment-related lymphopenia in patients with malignant gliomas: modeling radiation dose to circulating lymphocytes explains clinical observations and suggests methods of modifying the impact of radiation on immune cells. *Cancer Invest* 2013;31(2):140-4. doi: 10.3109/07357907.2012.762780 [published Online First: 2013/02/01]

23. Heylmann D, Ponath V, Kindler T, et al. Comparison of DNA repair and radiosensitivity of different blood cell populations. *Sci Rep* 2021;11(1):2478. doi: 10.1038/s41598-021-81058-1 [published Online First: 2021/01/30]
24. Kim YE, Gwak SH, Hong BJ, et al. Effects of Ultra-high doserate FLASH Irradiation on the Tumor Microenvironment in Lewis Lung Carcinoma: Role of Myosin Light Chain. *Int J Radiat Oncol Biol Phys* 2021;109(5):1440-53. doi: 10.1016/j.ijrobp.2020.11.012 [published Online First: 2020/11/14]
25. Alaghband Y, Cheeks SN, Allen BD, et al. Neuroprotection of Radiosensitive Juvenile Mice by Ultra-High Dose Rate FLASH Irradiation. *Cancers (Basel)* 2020;12(6) doi: 10.3390/cancers12061671 [published Online First: 2020/07/01]
26. Zhang Y, Ding Z, Perentesis JP, et al. Can Rational Combination of Ultra-high Dose Rate FLASH Radiotherapy with Immunotherapy Provide a Novel Approach to Cancer Treatment? *Clin Oncol (R Coll Radiol)* 2021;33(11):713-22. doi: 10.1016/j.clon.2021.09.003 [published Online First: 2021/09/24]
27. Iturri L, Bertho A, Lamirault C, et al. Proton FLASH Radiation Therapy and Immune Infiltration: Evaluation in an Orthotopic Glioma Rat Model. *Int J Radiat Oncol Biol Phys* 2023;116(3):655-65. doi: 10.1016/j.ijrobp.2022.12.018 [published Online First: 2022/12/24]
28. Cordero FJ, Huang Z, Grenier C, et al. Histone H3.3K27M Represses p16 to Accelerate Gliomagenesis in a Murine Model of DIPG. *Mol Cancer Res* 2017;15(9):1243-54. doi: 10.1158/1541-7786.MCR-16-0389 [published Online First: 2017/05/20]
29. Garty G, Obaid R, Deoli N, et al. Ultra-high dose rate FLASH irradiator at the radiological research accelerator facility. *Sci Rep* 2022;12(1):22149. doi: 10.1038/s41598-022-19211-7 [published Online First: 2022/12/23]
30. Yeo AT, Rawal S, Delcuze B, et al. Single-cell RNA sequencing reveals evolution of immune landscape during glioblastoma progression. *Nat Immunol* 2022;23(6):971-84. doi: 10.1038/s41590-022-01215-0 [published Online First: 20220527]
31. Kamran N, Kadiyala P, Saxena M, et al. Immunosuppressive Myeloid Cells' Blockade in the Glioma Microenvironment Enhances the Efficacy of Immune-Stimulatory Gene Therapy. *Mol Ther* 2017;25(1):232-48. doi: 10.1016/j.ymthe.2016.10.003 [published Online First: 20170104]
32. Ochocka N, Segit P, Walentynowicz KA, et al. Single-cell RNA sequencing reveals functional heterogeneity of glioma-associated brain macrophages. *Nat Commun* 2021;12(1):1151. doi: 10.1038/s41467-021-21407-w [published Online First: 20210219]
33. Hickman SE, Kingery ND, Ohsumi TK, et al. The microglial sensome revealed by direct RNA sequencing. *Nat Neurosci* 2013;16(12):1896-905. doi: 10.1038/nn.3554 [published Online First: 2013/10/29]
34. Keren-Shaul H, Spinrad A, Weiner A, et al. A Unique Microglia Type Associated with Restricting Development of Alzheimer's Disease. *Cell* 2017;169(7):1276-90 e17. doi: 10.1016/j.cell.2017.05.018 [published Online First: 2017/06/13]
35. Kumar A, Ghosh S, Chandna S. Evidence for microRNA-31 dependent Bim-Bax interaction preceding mitochondrial Bax translocation during radiation-induced apoptosis. *Sci Rep* 2015;5:15923. doi: 10.1038/srep15923 [published Online First: 2015/10/31]
36. Osman AM, Sun Y, Burns TC, et al. Radiation Triggers a Dynamic Sequence of Transient Microglial Alterations in Juvenile Brain. *Cell Rep* 2020;31(9):107699. doi: 10.1016/j.celrep.2020.107699 [published Online First: 2020/06/04]
37. Shi H, Sheng B, Zhang C, et al. Myeloid Kruppel-like factor 2 deficiency exacerbates neurological dysfunction and neuroinflammation in a murine model of multiple sclerosis. *J Neuroimmunol* 2014;274(1-2):234-9. doi: 10.1016/j.jneuroim.2014.06.023 [published Online First: 2014/07/24]

38. Merah-Mourah F, Cohen SO, Charron D, et al. Identification of Novel Human Monocyte Subsets and Evidence for Phenotypic Groups Defined by Interindividual Variations of Expression of Adhesion Molecules. *Sci Rep* 2020;10(1):4397. doi: 10.1038/s41598-020-61022-1 [published Online First: 2020/03/12]
39. Crane MJ, Daley JM, van Houtte O, et al. The monocyte to macrophage transition in the murine sterile wound. *PLoS One* 2014;9(1):e86660. doi: 10.1371/journal.pone.0086660 [published Online First: 2014/01/28]
40. Patil NS, Nabet BY, Muller S, et al. Intratumoral plasma cells predict outcomes to PD-L1 blockade in non-small cell lung cancer. *Cancer Cell* 2022;40(3):289-300 e4. doi: 10.1016/j.ccell.2022.02.002 [published Online First: 2022/02/27]
41. Hammond TR, Dufort C, Dissing-Olesen L, et al. Single-Cell RNA Sequencing of Microglia throughout the Mouse Lifespan and in the Injured Brain Reveals Complex Cell-State Changes. *Immunity* 2019;50(1):253-71 e6. doi: 10.1016/j.immuni.2018.11.004 [published Online First: 2018/11/26]
42. Lee PY, Li Y, Kumagai Y, et al. Type I interferon modulates monocyte recruitment and maturation in chronic inflammation. *Am J Pathol* 2009;175(5):2023-33. doi: 10.2353/ajpath.2009.090328 [published Online First: 2009/10/08]
43. Simmons DA, Lartey FM, Schuler E, et al. Reduced cognitive deficits after FLASH irradiation of whole mouse brain are associated with less hippocampal dendritic spine loss and neuroinflammation. *Radiother Oncol* 2019;139:4-10. doi: 10.1016/j.radonc.2019.06.006 [published Online First: 20190625]
44. Rama N ST, Shukla S, Goda C, Milewski D, Mascia AE, Vatner RE, Sengupta D, Katsis A, Abel E, Girdhani S, Miyazaki M, Rodriguez A, Ku A, Dua R, Parry R, Kalin TV. Improved Tumor Control Through T-cell Infiltration Modulated by Ultra-High Dose Rate Proton FLASH Using a Clinical Pencil Beam Scanning Proton System. *International Journal of Radiation Oncology, Biology, Physics* 2019;105(1):S164-S65. doi: https://doi.org/10.1016/j.ijrobp.2019.06.187
45. Lovatt M, Filby A, Parravicini V, et al. Lck regulates the threshold of activation in primary T cells, while both Lck and Fyn contribute to the magnitude of the extracellular signal-related kinase response. *Mol Cell Biol* 2006;26(22):8655-65. doi: 10.1128/MCB.00168-06 [published Online First: 2006/09/13]
46. Szabo PA, Levitin HM, Miron M, et al. Single-cell transcriptomics of human T cells reveals tissue and activation signatures in health and disease. *Nat Commun* 2019;10(1):4706. doi: 10.1038/s41467-019-12464-3 [published Online First: 2019/10/19]
47. Nishiga Y, Drainas AP, Baron M, et al. Radiotherapy in combination with CD47 blockade elicits a macrophage-mediated abscopal effect. *Nat Cancer* 2022;3(11):1351-66. doi: 10.1038/s43018-022-00456-0 [published Online First: 2022/11/22]
48. Wang Y, Johnson KCC, Gatti-Mays ME, et al. Emerging strategies in targeting tumor-resident myeloid cells for cancer immunotherapy. *J Hematol Oncol* 2022;15(1):118. doi: 10.1186/s13045-022-01335-y [published Online First: 2022/08/29]
49. Zhang P, Miska J, Lee-Chang C, et al. Therapeutic targeting of tumor-associated myeloid cells synergizes with radiation therapy for glioblastoma. *Proc Natl Acad Sci U S A* 2019;116(47):23714-23. doi: 10.1073/pnas.1906346116 [published Online First: 2019/11/13]
50. Walter AW, Mulhern RK, Gajjar A, et al. Survival and neurodevelopmental outcome of young children with medulloblastoma at St Jude Children's Research Hospital. *J Clin Oncol* 1999;17(12):3720-8. doi: 10.1200/JCO.1999.17.12.3720 [published Online First: 1999/11/30]

MAIN FIGURE LEGENDS

Figure 1: Experimental design and clustering of CD45+ cells. (a) Day 0; DMG cells are stereotactically injected into the brainstem of juvenile mice. 10 days post injection (dpi); tumor presence is confirmed by MRI. 17 dpi; mice are randomly assigned to receive either conventional radiation (RT) (CONV, 15Gy at 2Gy/min), FLASH (15Gy at 90Gy/sec), or no RT (Tumor). 21 dpi (4 days post-RT); all groups – including a Normal Brainstem cohort - are euthanized for cell isolation, hashtag oligonucleotide (HTO) staining, CD45+ sorting, and finally, single-cell RNA sequencing (scRNA-seq). **(b)** Clustering of 33,308 CD45+ cells reveals 17 unique cell subsets. **(c)** Cluster proportions by treatment group evaluated against the total number of cells collected for that specific group. **(d)** Key marker genes for each cluster.

Figure 2: Immune cell differences comparing CONV, FLASH and Tumor groups at day 4 (D4) and day 10 (D10) post-RT by flow cytometry. (a) Percent of microglia (MG) per CD45+ cells. **(b)** Percent of macrophages (MACs) per CD45+ cells. **(c)** Percent of myeloid derived suppressor cells (MDSCs) per CD45+ cells. **(d)** Percent of dendritic cells (DCs) per CD45+ cells. **(e)** Percent of T-cells per CD45+ cells. **(f)** Percent of CD8+ T-cells per CD45+ cells. **(g)** Percent of CD4+ T-cells per CD45+ cells. **(h)** Percent of CD19+ B-cells per CD45+. Statistical data available in Supplemental Data 2 with significant p-values considered as $p \leq 0.05$ highlighted in green.

Figure 3: Characterization and localization of MG subtypes across treatment groups. (a) Heatmap of top marker genes from each MG cluster. Feature plot of average expression of **(b)** P2ry12 and Apoe **(c)** Ifit3 and Isg15 and **(d)** Lpl and Fabp5 across the MG clusters. **(e)** Density of cells from each treatment group visualized across MG clusters. **(f)** MG cluster proportions within each treatment group, determined as the fraction of MG subtype cells over the total number of MG cells collected for that specific group.

Figure 4: Comparison of immune responses post FLASH and CONV in MACs. (a) Common up- and down-regulated genes between independent differential expression analyses of CONV vs Tumor (white) and FLASH vs Tumor (green) in the MAC cluster, plotted by average log2 fold change. **(b)** Volcano plot of the upregulated genes in CONV vs Tumor (left) and FLASH vs Tumor (right) in the MAC cluster. Gray vertical lines indicate average log2 fold change of 0.8 and horizontal gray line indicates adjusted p-value <0.05. **(c)** Density of cells from CONV and FLASH visualized across non-resident myeloid clusters (top). Feature plots of the average expression of top upregulated genes in CONV vs Tumor (bottom left) and FLASH vs Tumor (bottom right) across non-resident myeloid clusters. **(d)** ssGSEA analysis of MACs from CONV, FLASH and Tumor groups using REACTOME interferon alpha/beta gene set (IFN1). **(e)** Percent of IFNAR+ cells per MACs in CONV, FLASH, and Tumor groups at D4 and D10 post-RT. Statistical data available for flow cytometry in Supplemental Data 2. Significant p-values considered as $p \leq 0.05$.

Figure 5: Comparison of immune responses post FLASH and CONV in DCs. (a) Dot plot of top 20 most upregulated genes in CONV vs Tumor and the two significantly upregulated genes in FLASH vs Tumor in DCs. **(b)** ssGSEA analysis of IFN1 in DCs from CONV, FLASH and Tumor groups. **(c)** Percent of IFNAR+ cells per DCs in CONV, FLASH, and Tumor groups at

D4 and D10. Statistical data available for flow cytometry in Supplemental Data 2. Significant p-values considered as $p \leq 0.05$.

Figure 1

a

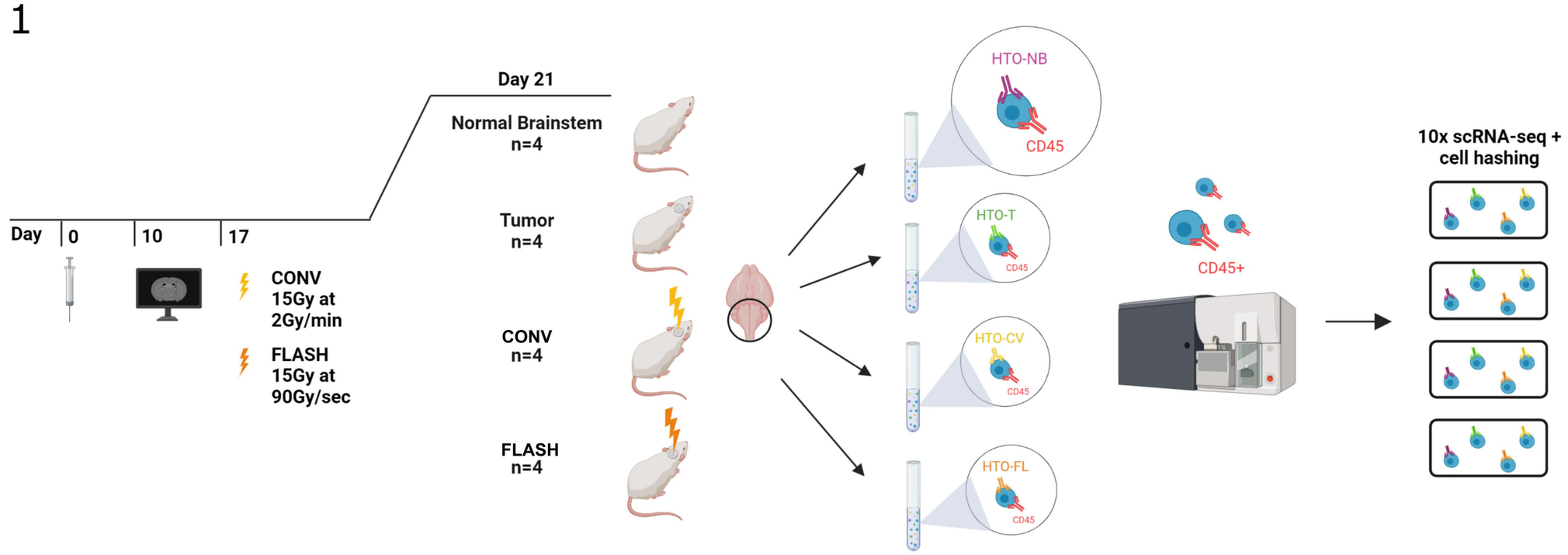

b

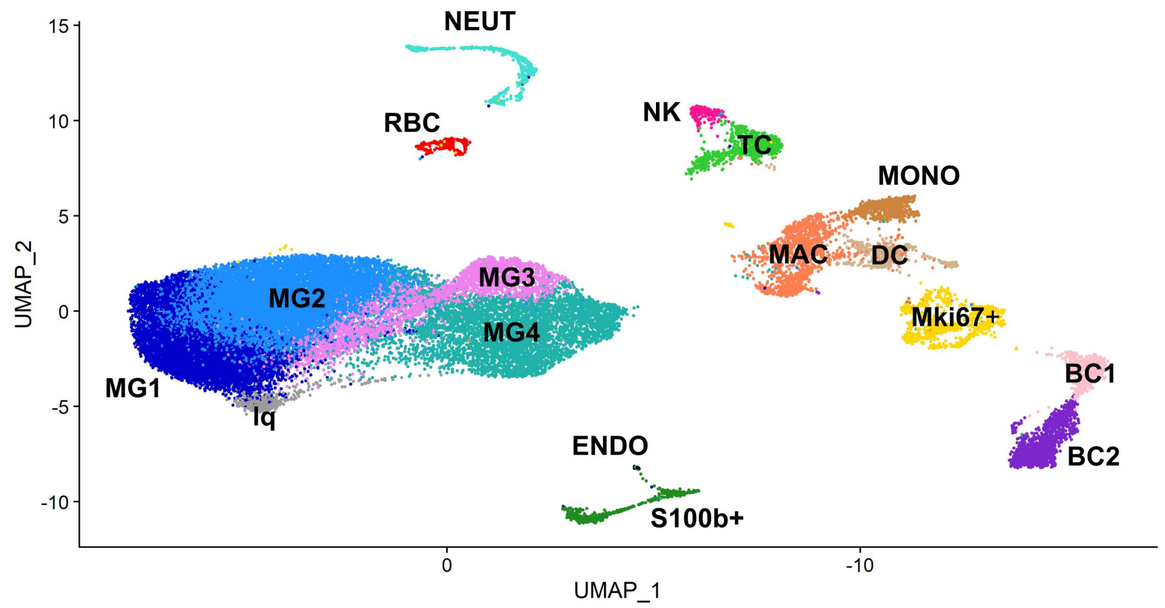

c

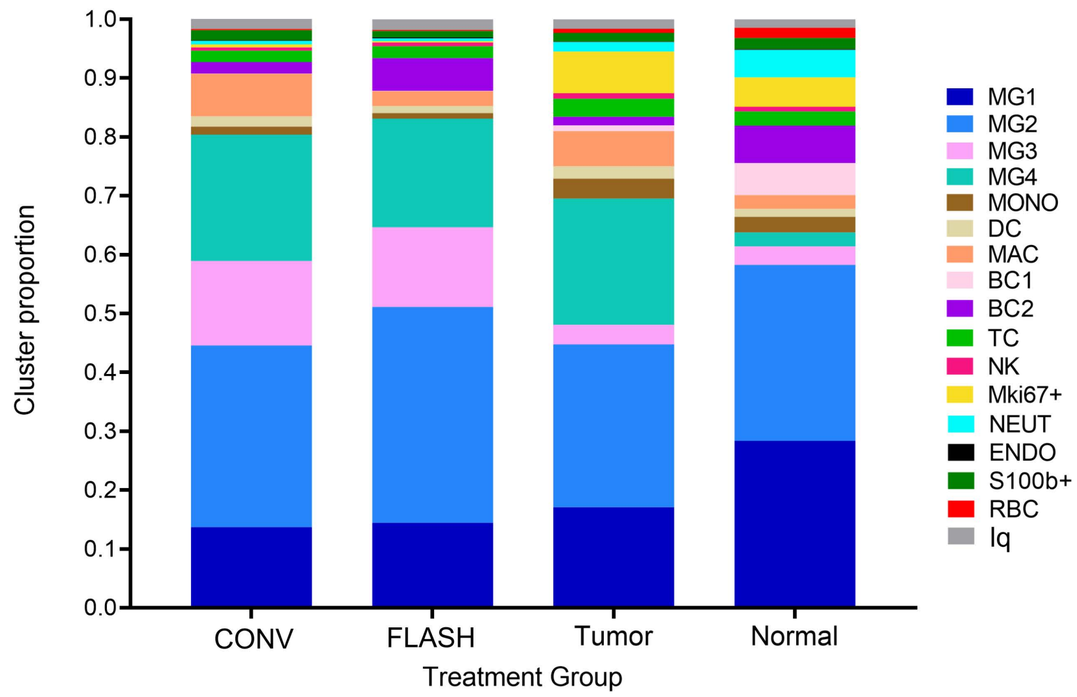

d

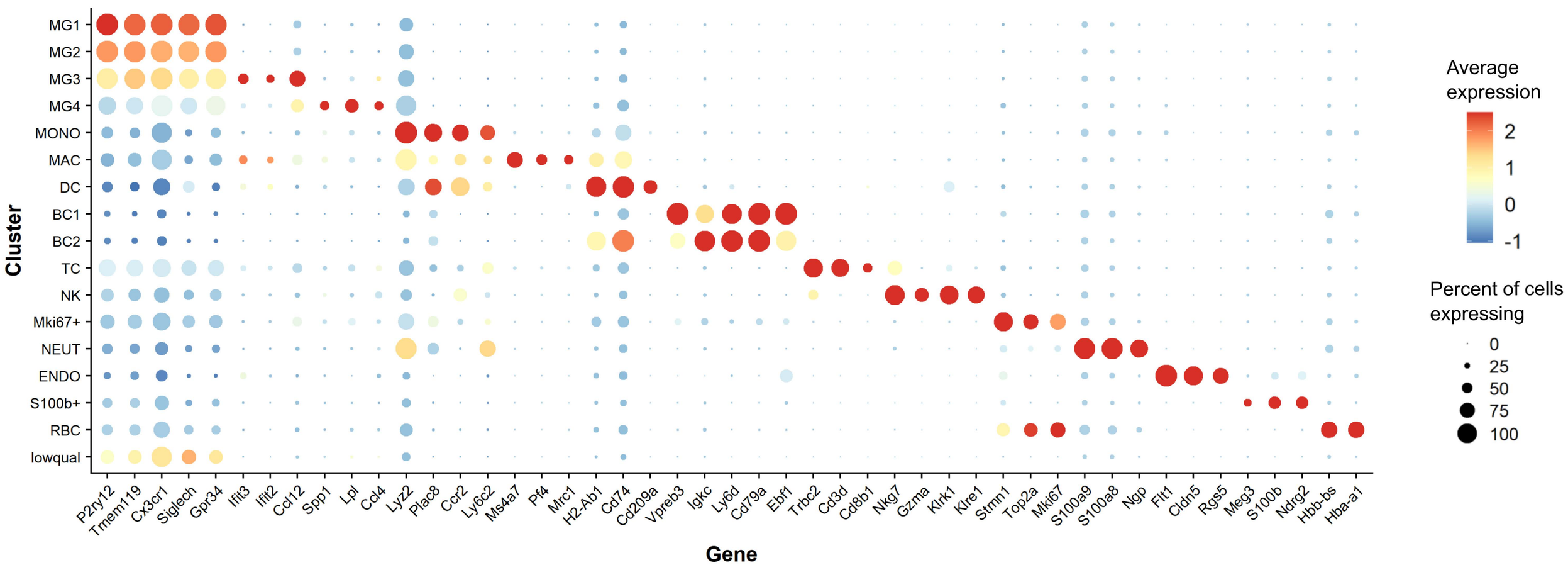

Figure 2

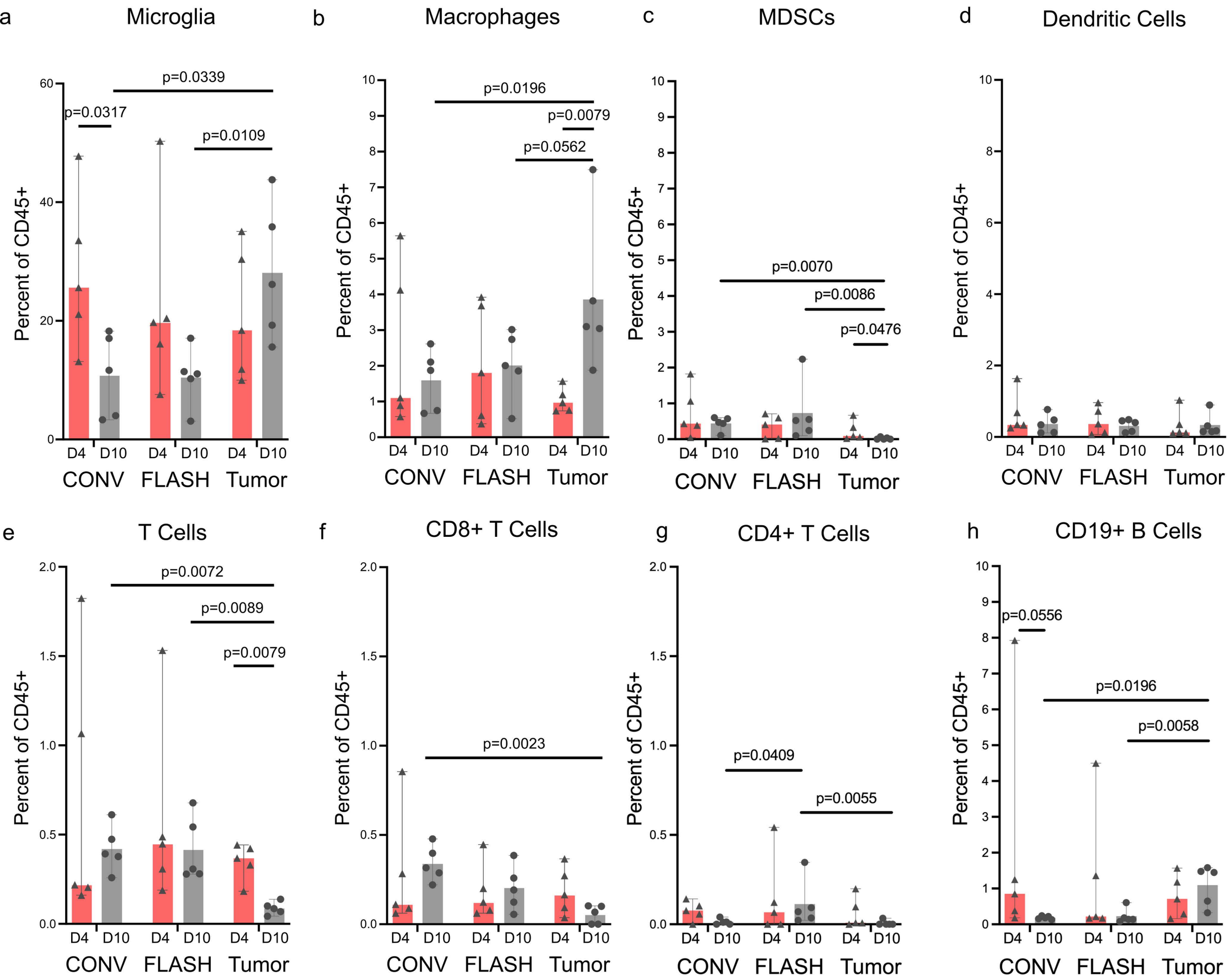
a
Microglia
p=0.0339
p=0.0317
p=0.0109
Percent of CD45+
D4 D10 D4 D10 D4 D10
CONV FLASH Tumor
b
Macrophages
p=0.0196
p=0.0079
p=0.0562
c
MDSCs
p=0.0070
p=0.0086
p=0.0476
d
Dendritic Cells
e
T Cells
p=0.0072
p=0.0089
p=0.0079
f
CD8+ T Cells
p=0.0023
g
CD4+ T Cells
p=0.0409
p=0.0055
h
CD19+ B Cells
p=0.0556
p=0.0196
p=0.0058

Figure 3

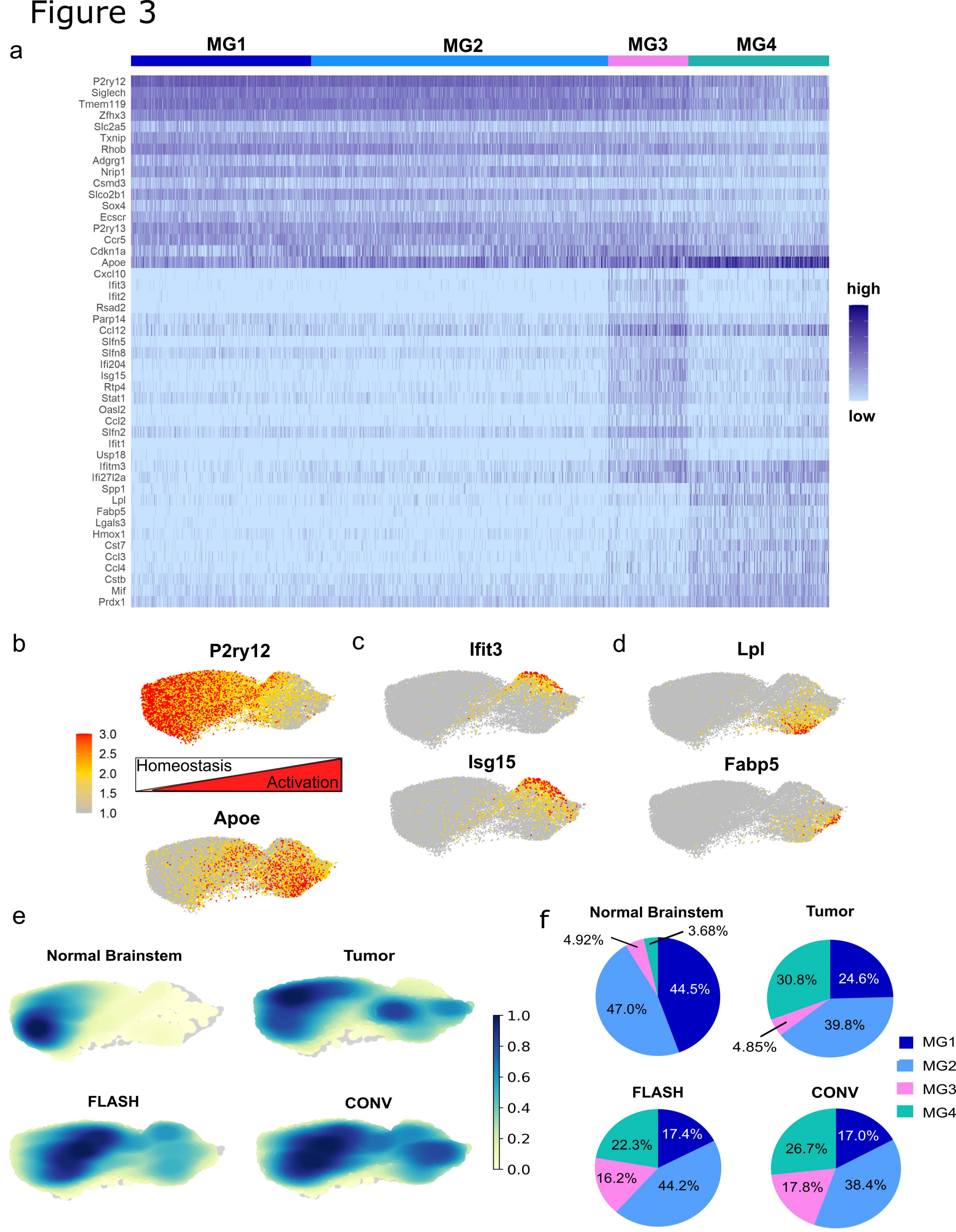
a
MG1
MG2
MG3
MG4
P2ry12
Siglech
Tmem119
Zfhx3
Slc2a5
Txnip
Rhob
Adgrg1
Nrip1
Csmd3
Slco2b1
Sox4
Ecscr
P2ry13
Ccr5
Cdkn1a
Apoe
Cxcl10
Ifit3
Ifit2
Rsad2
Parp14
Ccl12
Slfn5
Slfn8
Ifi204
Isg15
Rtp4
Stat1
Oasl2
Ccl2
Slfn2
Ifit1
Usp18
Ifitm3
Ifi27l2a
Spp1
Lpl
Fabp5
Lgals3
Hmox1
Cst7
Ccl3
Ccl4
Cstb
Mif
Prdx1
high
low
b
P2ry12
3.0
2.5
2.0
1.5
1.0
Homeostasis
Activation
Apoe
c
Ifit3
Isg15
d
Lpl
Fabp5
e
Normal Brainstem
Tumor
FLASH
CONV
1.0
0.8
0.6
0.4
0.2
0.0
f
Normal Brainstem
4.92%
3.68%
44.5%
47.0%
Tumor
30.8%
24.6%
39.8%
4.85%
FLASH
22.3%
17.4%
16.2%
44.2%
CONV
26.7%
17.0%
17.8%
38.4%
MG1
MG2
MG3
MG4

Figure 4

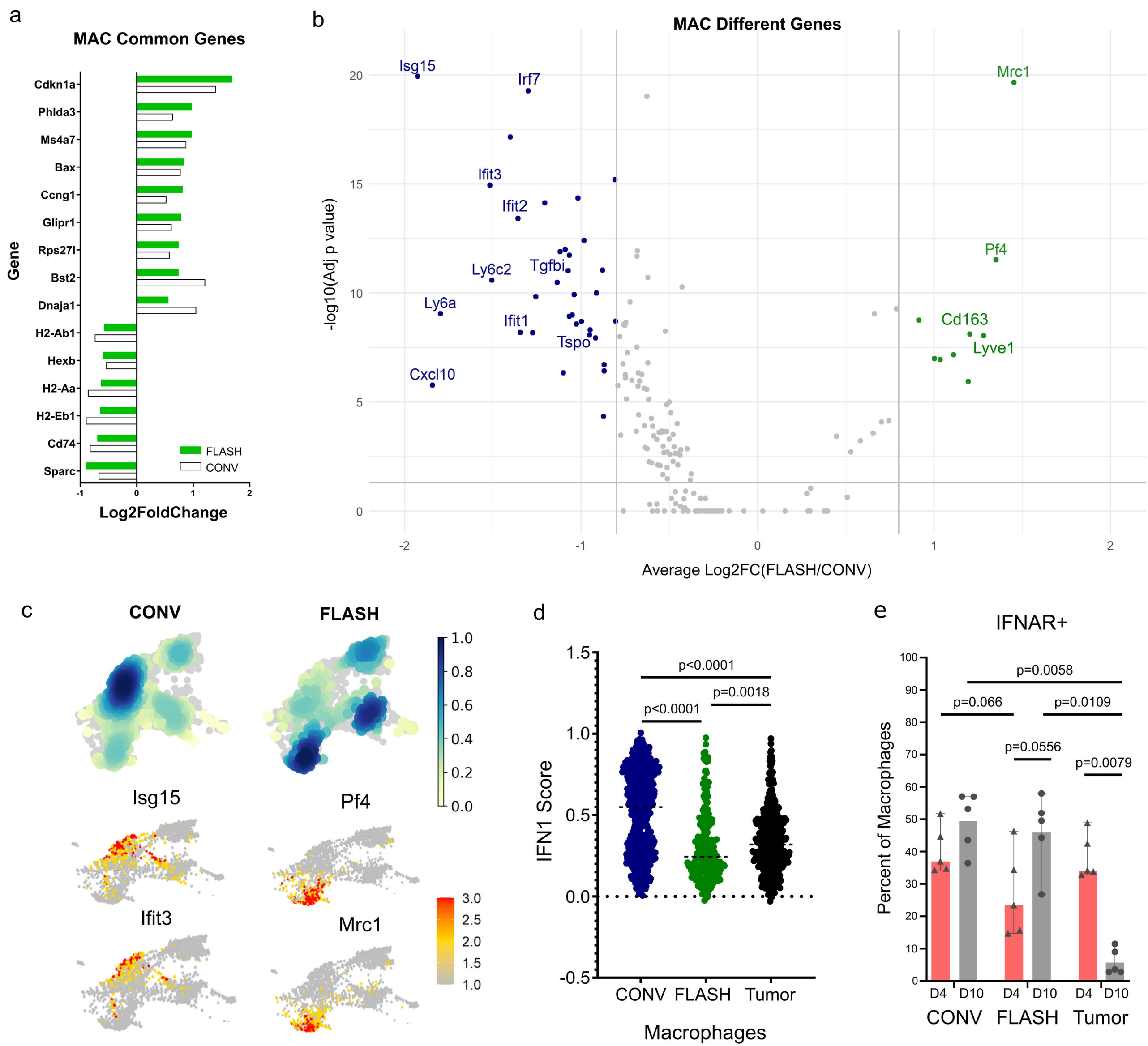
a
MAC Common Genes
Cdkn1a
Phlda3
Ms4a7
Bax
Ccng1
Glipr1
Rps27l
Bst2
Dnaja1
H2-Ab1
Hexb
H2-Aa
H2-Eb1
Cd74
Sparc
Gene
FLASH
CONV
-1
0
1
2
Log2FoldChange
b
MAC Different Genes
Isg15
Irf7
Ifit3
Ifit2
Ly6c2
Tgfbi
Ly6a
Ifit1
Tspo
Cxcl10
Mrc1
Pf4
Cd163
Lyve1
-log10(Adj p value)
20
15
10
5
0
-2
-1
0
1
2
Average Log2FC(FLASH/CONV)
c
CONV
FLASH
1.0
0.8
0.6
0.4
0.2
0.0
Isg15
Pf4
Ifit3
Mrc1
3.0
2.5
2.0
1.5
1.0
d
1.5
1.0
0.5
0.0
-0.5
IFN1 Score
p<0.0001
p=0.0018
p<0.0001
CONV
FLASH
Tumor
Macrophages
e
IFNAR+
100
90
80
70
60
50
40
30
20
10
0
Percent of Macrophages
p=0.0058
p=0.066
p=0.0109
p=0.0556
p=0.0079
D4
D10
D4
D10
D4
D10
CONV
FLASH
Tumor

Figure 5

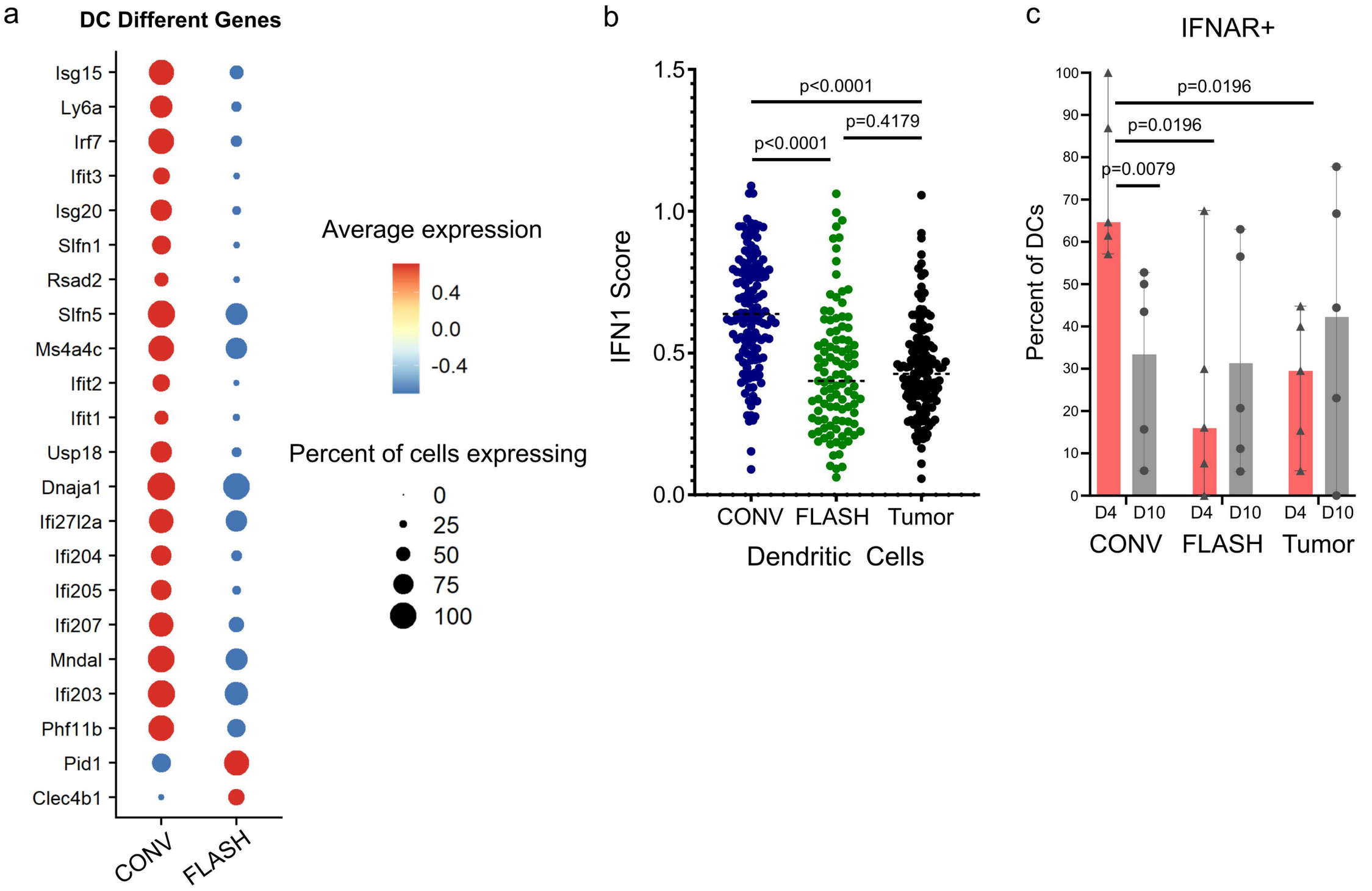
a
DC Different Genes
Isg15
Ly6a
Irf7
Ifit3
Isg20
Slfn1
Rsad2
Slfn5
Ms4a4c
Ifit2
Ifit1
Usp18
Dnaja1
Ifi27l2a
Ifi204
Ifi205
Ifi207
Mndal
Ifi203
Phf11b
Pid1
Clec4b1
CONV
FLASH
Average expression
0.4
0.0
-0.4
Percent of cells expressing
0
25
50
75
100
b
IFN1 Score
1.5
1.0
0.5
0.0
p<0.0001
p=0.4179
p<0.0001
CONV
FLASH
Tumor
Dendritic Cells
c
IFNAR+
Percent of DCs
100
90
80
70
60
50
40
30
20
10
0
p=0.0196
p=0.0196
p=0.0079
D4
D10
D4
D10
D4
D10
CONV
FLASH
Tumor